5th ECPMG Delft · 2024

Proceedings of the 5th ECPMG 2024
5th European Conference on Physical Modelling in Geotechnics
2-4 October 2024, Delft, the Netherlands

Centrifuge-Based Physical Modeling of Reinforced Concrete Using 3D Printed Reinforcement Cages

M. Elmorsy
Institute of Structural Engineering, ETH Zürich, Zürich, Switzerland, medhat.elmorsy@ibk.baug.ethz.ch

R. Wrobel
EMPA, Swiss Federal Laboratories for Materials Science and Technology, Dübendorf, Switzerland

C. Leinenbach
EMPA, Swiss Federal Laboratories for Materials Science and Technology, Dübendorf, Switzerland

Laboratory for Photonic Materials and Characterization, École Polytechnique Fédérale de Lausanne (EPFL), Lausanne, Switzerland

M.F. Vassiliou
Institute of Structural Engineering, ETH Zürich, Zürich, Switzerland, vassiliou@ibk.baug.ethz.ch

ABSTRACT: Small-scale physical models for use in shake table centrifuge testing are useful both to geotechnical and structural engineers. At scales on the order of 1:40 creating physical models of Reinforced Concrete (RC) structures presents manufacturing difficulties, as it is hard and time-consuming to build and place such small rebars. This paper shows that the steel reinforcement can be 3D printed in the form of reinforcing cages, even at submillimeter diameters. It discusses quasi-static cyclic tests on cantilever columns and beam-column joints with different configurations. The findings suggest that the behavior of the tested small-scale RC components mirrors that of their full-scale counterparts. This similarity implies that such 1:40 specimens hold promise as a physical modeling approach for centrifuge testing.

1 INTRODUCTION

Small-scale physical models play a crucial role in geotechnical and structural engineering for two main reasons, as highlighted by Del Giudice et al. (2022). Firstly, these models find application in centrifuge studies of Soil-Structure Interaction (SSI) problems, where such reduced scales are typical. Secondly, addressing the challenges faced by numerical models in accurately predicting the shake table response of structures requires a focus on system-level testing. Researchers (Bradley, 2013; Zhang et al., 2023) have identified a significant source of error at the system level, emphasizing the importance of the "overall modeling methodology" in numerical models.

Given the lack of extensive experimental data at the system level, especially involving costly tests of whole structures on a shake table, validating numerical models becomes challenging. Consequently, low-cost small-scale tests become valuable for validating system-level assumptions, including how components interact and how the global damping matrix should be formulated, despite the scale dependency of concrete mechanical properties (Harris and Sabnis, 1999).

While acknowledging the distortion inherent in 1:30/1:40 models due to scale-dependent concrete properties, the primary aim is not to create undistorted models. Instead, the focus is on statistically validating global assumptions based on experimentally obtained component-level behavior at the model scale. Such statistical validation was employed by several researchers in earthquake engineering (Bachmann et al., 2018; Vassiliou et al., 2021; Elmorsy and Vassiliou, 2023). Thus, the pursuit of physically modeling structures at such small scales is justified, especially in geotechnical engineering where centrifuge modeling is crucial for maintaining stress similitude. Traditional challenges in creating small-scale models, such as those faced by Knappett et al. (2011), led to limitations, including difficulties in accurate positioning of handmade micro-reinforcement and extended construction times.

To overcome these challenges, Del Giudice et al. (2022) explored using a metal 3D printer for manufacturing the reinforcement of 1:40 scaled models. This involved employing fine silica sand as aggregate and either cement or gypsum as a binder. The 3D-printed steel reinforced columns tested under

cyclic loads closely resembled the behavior of full-scale columns, offering a feasible approach. However, their study had limitations, such as the challenges in replicating post-peak degradation behavior in numerical analyses, due to unexpected fracture of the reinforcement.

Continuing efforts by Elmorsy et al. (2023; 2024) focused on material and component level tests at the model scale, including axial loads in RC column tests. These efforts demonstrated adjustability in 3D printed steel mechanical properties, suitable concrete properties, reasonable bond behavior, and comparable failure modes to full-scale cyclic tests of RC columns, providing valuable insights for structural and geotechnical applications. Using small scale factors (e.g., 1:100) is currently not possible mainly due to 3D printers accuracy and the difficulties in the fact that concrete is still cast manually. Future development in 3D printing technologies may allow for such small scales.

This paper discusses quasi-static cyclic tests on columns and beam-column joints with different configurations. The experiments are compared to numerical models implemented in Opensees.

2 EXPERIMENTAL CAMPAIGN

2.1 Specimen details and manufacturing

The tested specimens (three specimens) were based on a 1:30 scaled model of a seismically designed two-story RC building. Figure 1 depicts the geometry and reinforcement details for the tested specimens including column, exterior, and knee beam-column joints. Foundation, beam, and column cages were printed separately and then assembled manually together in the formwork. However, it is important to highlight that the entire cage for each element (beam or column cage) was printed as a single unit, requiring a degree of continuity in both longitudinal rebars and stirrups. This continuous arrangement simplifies the 3D printing process, as printing stirrups passing outside the longitudinal reinforcement or producing separate hoops and cross ties would have been impractical. While additive manufacturing technology is rapidly advancing, enabling the potential for printing more intricate geometries in the future, the suggested method could be expanded or refined.

In exterior and knee joints, the beam reinforcement was anchored in the beam-column joint region using headed bars. This was driven by the need to have an easy-to-assemble reinforcement layout since the assembly was done manually.

Figure 2a shows the 3D printed parts (reinforcement cages) right after finishing the print job. It also shows the printing direction (45 degrees from the build plate). A support structure was printed since 3D printers cannot easily print “overhanging elements”, i.e. horizontal elements that are not supported (Figure 2a). A PLA (Polylactic acid) 3D printer was used to print the molds for accurate dimensioning of the specimens (Figure 2b). After casting and curing, the specimens were painted using white paint and then a speckle pattern was applied to the specimens as preparation for DIC measurements using an airbrush (Figure 2c).

2.2 Materials

Elmorsy et al. (2023; 2024) and Knappett et al. (2011) explored various concrete mixes with cement and gypsum as binders. Their findings favored a gypsum-based model concrete over cement-based mixes for its closer similarity to prototype concrete, particularly in tensile strength. Consequently, a gypsum-based model concrete with a sand/water/binder ratio of 1/1/0.7 by weight was chosen for the current study. The chosen gypsum was a standard molding gypsum (named Prestia Tradition Plaster), and Perth silica sand (Crystalline silica SiO2) with a d_{50} = 0.23 mm was used. The grain distribution of this sand aligns well with the typical aggregate size when scaled 30-40 times (Del Giudice et al. 2022).

Uniaxial compression tests were conducted on cylinders (diameter 15 mm, height 30 mm), and four-point bending tests were performed on beams (15 mm x 15 mm cross-section, 80 mm length, shear span of 20 mm). Table 1 presents the average uniaxial compressive strength (f_c) and modulus of rupture (f_r) for these specimens, reflecting an average of five samples.

For steel reinforcement bars, gas-atomized 316L stainless steel powder with a particle size distribution of 45 ± 15µm was used (provider: Oerlikon AM). These rebars were fabricated using a Concept Laser M2 L-PBF machine, employing a 200 W 1070 nm fiber laser. The build volume comprises a 245 x 245 mm build plate and a 285 mm maximum build height. The mechanical properties of the 3D-printed submillimeter rebars were adjusted by modifying the printing parameters and are reported in Table 1 (the average yield strength (f_y) and ultimate strength (f_u)). Laser power, scanning speed, layer thickness, and hatch spacing were set at 110 W, 300 mm/s, 0.03 mm, and 0.01 mm, respectively. All bars were fabricated inclined at 45° concerning the base plate to fit as big

as possible samples (Figure 2a). Moreover, a support structure was used to dissipate the heat produced

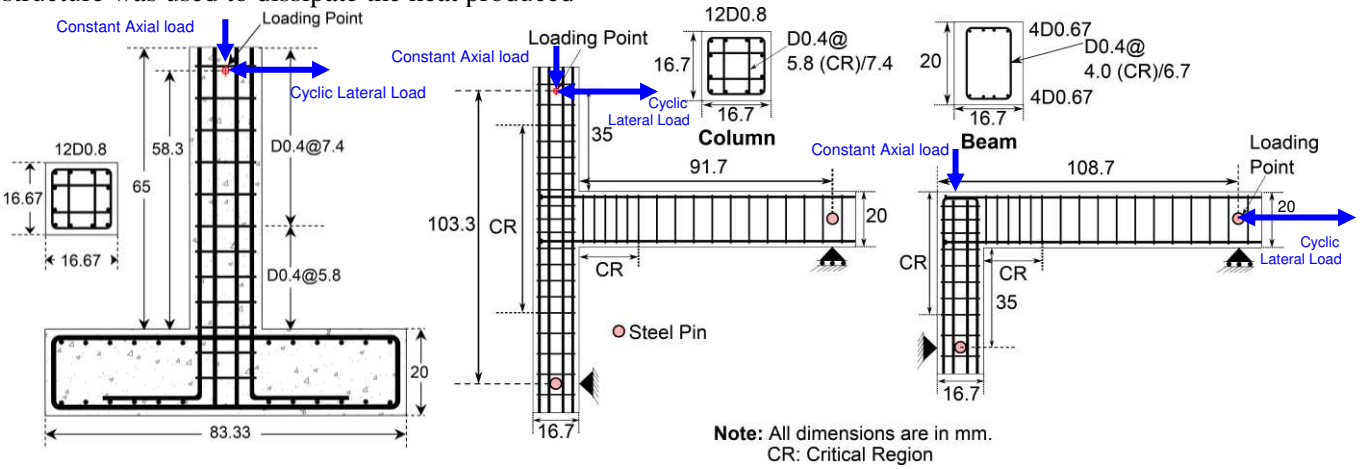

Figure 1. Specimen details: (left) Column, (middle) Exterior beam-column joint, and (right) Knee beam-column joint.

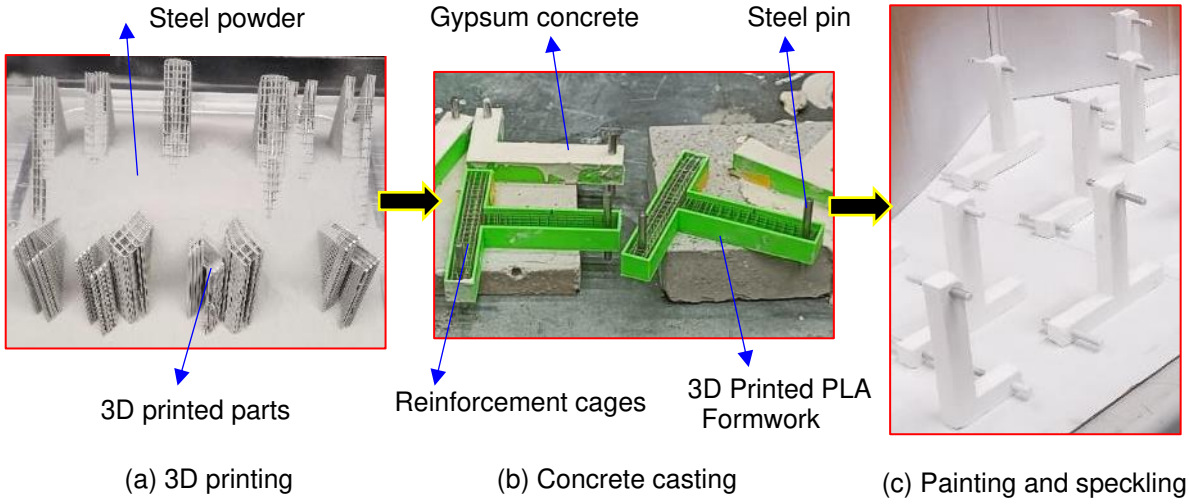

Figure 2. Specimen manufacturing process.

during laser processing into the build plate and to avoid any distortion of the parts during fabrication.

These printing parameters were chosen since they produced the closest mechanical properties compared to the recommendation of EC2 (CEN, 2004; Elmorsy et al. 2023). Surface ribs were printed on the rebars with specific parameters. Pullout tests of rebars with these surface rib parameters demonstrated bond-slip relationships comparable to full-scale relationships (Elmorsy et al., 2023).

Table 1. Material characteristics.

Specimen	f_c [MPa]	f_r [MPa]	f_y [MPa]	f_u [MPa]
Column	20.0	4.12	460.2	535.4
Exterior Joint	19.6	3.86	466.7 (439.8)*	573.1 (560.6)*
Knee Joint	20.0	3.99	466.7 (439.8)*	573.1 (560.6)*

*Beam (column)

Together with the tensile strength, the bond between the rebars and the concrete is of vital importance – if both are excessively high, it results in strain localization (compared to prototype concrete) and premature fracture of the rebars as was observed in the tests by (Del Giudice et al. 2022).

2.3 Test setup and loading protocol

The specimens underwent reversed lateral cyclic loading, in a setup that was accommodated in a 200 kN Universal Testing Machine (UTM). The lateral cyclic loading was implemented through the UTM actuator via loading pins connected to a double-hinged fork, which transferred the UTM-applied load to the specimens. No axial load was applied.

The adopted lateral loading protocol, comprises two displacement-controlled cycles per displacement amplitude, with amplitudes increasing by 40% relative to the preceding amplitude. To explore behavior before yielding, four displacement

amplitudes were applied at 0.25, 0.5, 0.75, and 1.00 times the yield drift. The yield drift ratio was defined as the drift causing the first yield of steel reinforcement using a fiber model of the column/joint in Opensees (Mazzoni et al., 2006). The drift ratio is defined as the column displacement divided by the height of the column from the support point to loading point in the column and exterior joint specimens. In the knee joint specimen, the height of the column calculated from the pin support to the centerline of the beam.

The applied cyclic load was measured using the UTM load cell. The displacement measuring system consists of two LVDTs that were mounted on the two sides of the loading pins and a 3D Digital Image Correlation (3D-DIC) system. The LVDTs measured the displacement of the cyclic load application point, while the DIC system captured displacements and strain fields. The strain distribution was used to identify any cracks and micro-cracks formed during the tests and to locate the plastic hinges that formed at the critical section of the beam. The specimens were prepared for DIC measurements by white-painting and subsequent speckling using an airbrush, as discussed earlier.

3 RESULTS AND DISCUSSION

3.1 Failure mode

The failure mode was observed by naked eye as well as using the high-quality photos generated using the DIC system. Figure 3 depicts the observed failure mode. The column specimens failed in flexural hinging mode. Figure 3 (left) shows the failure mode as observed at the end of the test for the column specimen. The failure involved fracture of the longitudinal reinforcement accompanied by bar buckling, concrete cover spalling, concrete crushing, and hoop yielding. Such a failure mode occurred at a zone close to the base cross-section. Micro-cracks were not visible to the naked eye because of the small scale of the specimens. However, DIC-based principal strain distribution at peak load showed that micro-cracks along the length of the column did form, which is similar to full-scale RC columns.

The exterior and knee joints (Figures 3 (middle) and Figure 3 (right), respectively) failed in beam flexural hinging mode. Such failure mode (often denoted: B-failure) is evident through the cracking pattern; having a major crack near the interface of the beam with the beam-column joint region and a few minor cracks that were distributed over a larger area of the beam near that interface. In B-failure mode, the longitudinal beam reinforcement reaches yield while joint shear strength is still higher than the joint shear stress demand.

3.2 Force-displacement relationship

The force-deformation relationships of the tested specimens are shown in Figure 4. In addition, Figure 4 also shows the envelope (backbone) curves that were developed by connecting the peak of the first cycle at each displacement (drift) level. The positive sign indicates the downward direction (the first loading direction) in the column and the exterior joint specimen and the opening moment direction for the knee joint.

The column specimen was able to reach high drift ratios (17%) without significant loss of load carrying capacity (70% strength loss at the end of the test) even after cover loss and bar buckling. This behavior is usually observed in full-scale columns. Despite the specimen being reinforced symmetrically, its force-deformation pattern was not perfectly symmetric. This observation aligns as well with findings from full-scale tests. For instance, Saatcioglu and Ozcebe (1989) reported unsymmetrical behavior in specimens tested under zero axial load. This asymmetry can be attributed to the variability in steel properties, as well as the Bauschinger effect and isotropic hardening of the steel during cyclic loading.

The exterior joint was able to reach a high drift ratio without significant loss of load-carrying capacity. The maximum reached drift ratio was 6.7% and 8.7% for the positive and negative directions, respectively. Post-peak strength maintaining was observed. This aligns well with full-scale exterior joints failing in B-failure mode (Elmorsy, 2020; Hassan and Elmorsy, 2022a). For knee joints, a high drift ratio was reached without significant loss of load-carrying capacity. The maximum reached drift ratio was 7.6% and 7.3% for positive and negative directions, respectively. Force-deformation curves were not symmetric, which aligns with full-scale tests and is due to the fact that the beam endures tension force during the opening moment while it endures compression during the closing moment (Ghimire 2018).

3.3 Numerical modeling

This section aims to show that numerical models developed for prototype RC components can describe the behavior of the tested specimens if their material- and component-level parameters are calibrated against the small-scale material and component tests. Accordingly, these models could be used in the future

to validate the system level assumptions against small-scale shake table tests.

Numerical models of the performed cyclic tests were developed using the Opensees platform (Mazzoni et al., 2006). Columns and beams were modeled using the forceBeamColumn line element with HingeRadau integration. Fiber sections were used to model the RC beam and column sections. Concrete01 uniaxial material was used to model concrete. The parameters for the unconfined concrete (cover concrete) were obtained from the material level tests on the small-scale specimens as discussed in section 2.2 of this paper, while the confined concrete (core) was calculated using Mander's model (Mander et al., 1988). The reinforcement was modeled using the HystereticSM model in Opensees. This model was chosen as it allows for a more general hysteretic response than typical Opensees steel material models (e.g., Steel01). The backbone parameters of steel material were based on the material tests discussed in section 2.2 while the cyclic deterioration parameters were manually calibrated to match the hysteretic behavior of the tested small-scale columns. The same cyclic degradation parameters were used for all the three specimens.

Beam-column joint deformations were modeled implicitly by adjusting a centerline model as recommended by Standard ACI 369-22 (2023). Implicit modeling means that joint shear deformations are not modeled using special additional elements such as rotational springs (explicit modeling), (Hassan and Elmorsy 2022b). In modern frame construction, where the strength of the connecting columns is larger than 120% of that of the connecting beams, such implicit modeling is performed by extending the beam element inside the joint region (until the joint center) and making the column offsets as rigid links.

Figure 5 compares the numerical models developed in Opensees to the experimental results. It shows good agreement between the experimental results and the Opensees models. This good alignment suggests that it is viable to use such modeling techniques to create system-level models, use them to explore different system-level assumptions and parameter values, and validate them against shake table tests of whole structures.

4 CONCLUSIONS

This paper explored the application of metal 3D printing to produce reinforcement for small-scale models (in this paper, 1:30 scale) of Reinforced Concrete (RC) structures. The focus is on conducting cyclic tests on small-scale RC joints, utilizing sub-millimeter diameter rebar cages. The study aims to assess the viability of 3D printing for creating such models, especially for applications like centrifuge testing in earthquake engineering. Experimental results are compared with numerical models developed in the Opensees platform and are employed for validation. The findings indicate the feasibility of 3D printing reinforcement cages for small-scale structures, and the Opensees model effectively replicates the observed cyclic behavior in experiments. This successful 3D printing process has the potential to extend to printing reinforcement for entire buildings or bridges, facilitating the testing of small-scale specimens representing complete RC structures within a centrifuge.

ACKNOWLEDGEMENTS

This work was supported by the ETH Zurich under grant ETH-11 21-1. The work of Mr. Andreas Alff, a lab technician at EMPA, in printing the reinforcement cages is greatly acknowledged. The help of Mr. Stefan Murer, Mr. Julian Schlachter, and Mr. Manuel Wild in conducting the joint tests as part of a semester project at ETH Zurich is greatly appreciated.

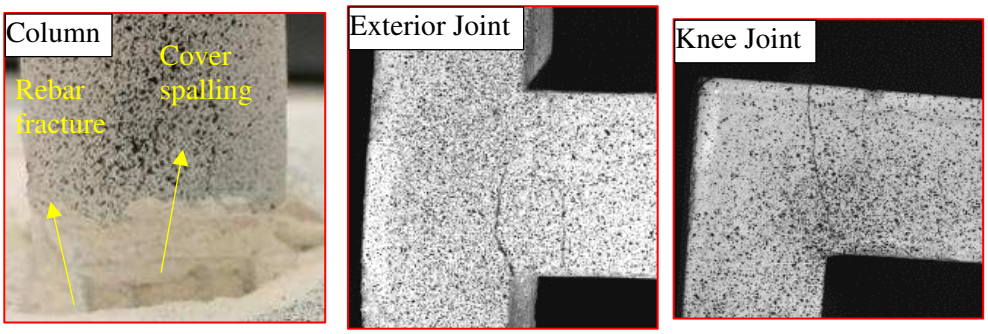

Figure 3. Failure mode of the specimens.

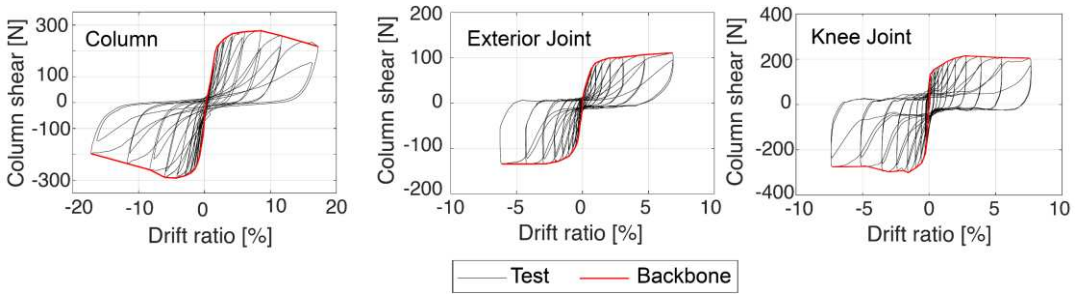

Figure 4. Force-deformation relationships.

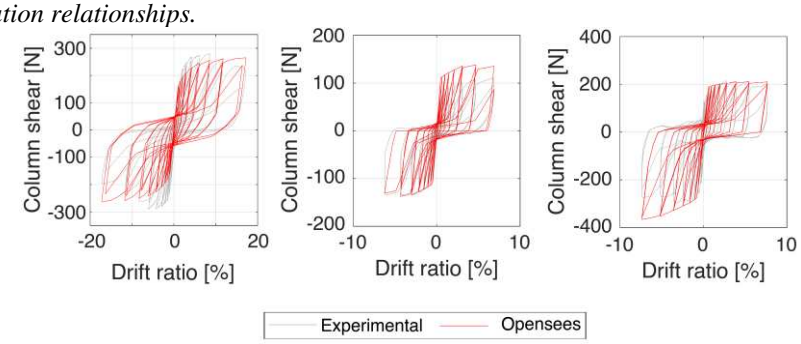

Figure 5. Numerical analysis results.

REFERENCES

American Concrete Institute, ACI (2023). *ACI 369-22: Standard Requirements for Seismic Evaluation and Retrofit of Existing Concrete Buildings*.

Bachmann, J.A., Strand, M., Vassiliou, M.F., Broccardo, M., and Stojadinović, B. (2018). Is rocking motion predictable?. *Earthquake Engineering & Structural Dynamics*, 47(2).

Bradley, B.A. (2013). A critical examination of seismic response uncertainty analysis in earthquake engineering. *Earthquake engineering & structural dynamics*, 42(11).

Del Giudice, L., Wróbel, R., Katsamakas, A., Leinenbach, C., and Vassiliou, M.F. (2022). Physical modelling of reinforced concrete at a 1: 40 scale using additively manufactured reinforcement cages. *Earthquake Engineering & Structural Dynamics*, 51(3), 537-551.

Elmorsy, M. (2020). *Nonlinear modeling parameters for beam-column joints in seismic analysis of concrete buildings*. Master Thesis, University of Alaska Anchorage, AK, USA.

Elmorsy, M., Wrobel, R., Leinenbach, C., and Vassiliou, M.F. (2024). Additively Manufactured Steel Reinforcement for Small Scale Reinforced Concrete Modeling: Tensile and Bond Behavior. *Materials and Design*, 241, 112919. https://doi.org/10.1016/j.matdes.2024.112919

Elmorsy, M. and Vassiliou, M.F. (2023). Effect of ground motion processing and filtering on the response of rocking structures. *Earthquake Engineering & Structural Dynamics*, 52(6), 1704-1721. https://doi.org/10.1002/eqe.3837

Elmorsy, M., Wrobel, R., Leinenbach, C., and Vassiliou, M.F. (2023). Material testing of micro-concrete and 3D-printed reinforcement for use in small-scale seismic testing of RC structures. *9th International Conference on Computational Methods in Structural Dynamics and Earthquake Engineering COMPDYN*, Athens, Greece.

European Committee for Standardisation (CEN) (2004). *Eurocode 2: Design of Concrete Structures. Part 1: General Rules and Rules for Buildings*.

Ghimire, K.P. (2018). *Anchorage of headed reinforcing bars in concrete*. Doctoral Thesis, University of Kansas.

Harris, H. G. and Sabnis, G. (1999). *Structural modeling and experimental techniques*. CRC press.

Hassan, W.M. and Elmorsy, M. (2022). Probabilistic Beam–Column Joint Model for Seismic Analysis of Concrete Frames. *Journal of Structural Engineering*, 148(4), 04022011.

Hassan, W.M. and Elmorsy, M., 2022. Cyclic nonlinear modeling parameters for unconfined beam-column joints. *ACI Struct. J*, 119(1), pp.89-104.

Knappett, J.A., Reid, C., Kinmond, S., and O'Reilly, K. (2011). Small-scale modeling of reinforced concrete structural elements for use in a geotechnical centrifuge. *Journal of Structural Engineering*, 137(11), 1263-1271.

Mander, J.B., Priestley, M. J., and Park, R. (1988). Theoretical stress-strain model for confined concrete. *Journal of structural engineering*, 114(8), 1804-1826.

Mazzoni S., McKenna F., Scott M.H., Fenves G.L. (2006). *OpenSees Command Language Manual*. University of California, Berkeley: Pacific Earthquake Engineering Research (PEER) Center.

Saatcioglu, M. and Ozcebe, G. (1989). Response of reinforced concrete columns to simulated seismic loading. *ACI Structural Journal*, 86(1), 3-12.

Vassiliou, M.F., Broccardo, M., Cengiz, C., Dietz, M., Dihoru, L., Gunay, S., ... and Stojadinovic, B. (2021). Shake table testing of a rocking podium: Results of a blind prediction contest. *Earthquake Engineering & Structural Dynamics*, 50(4), 1043-1062.

Zhang, H., Kwon, O.S., and Christopoulos, C. (2023). Hybrid-simulation-based model calibration method for nonlinear seismic analysis. *Earthquake Engineering & Structural Dynamics*.